Hindawi
Geofluids
Volume 2022, Article ID 3567816, 14 pages
https://doi.org/10.1155/2022/3567816

Research Article

Performance of Prestressed Anchor Cables Supporting Deep Foundation Pit of a Subway Station during Spring Thaw

Chuntao Feng,[1] **Zhihe Cheng**,[2] **and Lei Zhu**[2]

[1]*Institute of Environment Economics, Chinese Academy of Natural Resources Economics, Beijing 101149, China*
[2]*School of Civil Engineering, Harbin Institute of Technology, Harbin 150090, China*

Correspondence should be addressed to Zhihe Cheng; 17204054005@stu.xust.edu.cn

Received 19 October 2022; Revised 21 November 2022; Accepted 25 November 2022; Published 17 December 2022

Academic Editor: Xianwei Zhang

Based on the deep foundation pit for a subway station in Changchun (China), a 3D numerical model of water–heat coupling in a prestressed pile anchor system was established to determine its performance in freezing and thawing seasons in alpine areas. Its reliability was confirmed using field monitoring data on the prestressed anchor cables, which demonstrated changes in surface subsidence, anchor cable axial force, and pile horizontal displacement during spring thaw. The results demonstrated different degrees of elevation of the ground surface at the beginning of the spring thaw depending on whether the ground surface was at 2, 5, or 8 m from the pit excavation surface. Moreover, they demonstrated the occurrence of melting and surface subsidence when the temperature rises above 0°C, and that the axial force of the anchor cables fluctuates at the beginning of spring thaw but stabilizes in its middle and late stages. The phenomenon of pile horizontal displacement during the spring thaw could be roughly divided into three stages, with the second stage resulting in the most significant displacement. These results can provide certain reference for deep foundation pit projects in alpine areas.

1. Introduction

Because of the overall promotion of transportation, the development of highways and railways has rapidly developed, and the number of urban deep foundation pit projects has correspondingly increased. In China, frozen soil is widely distributed [1, 2]. In seasonally frozen soil areas, the foundation pit active layer of the soil experiences repeated freeze thaw action, considerably affecting the stability of related projects such as building sites and subway stations.

These freeze thaw cycles affect both the physical properties (pore ratio, water content, and permeability) and mechanical properties (cohesion, internal friction angle, elastic modulus, and damping ratio) of soil [3]. Zhang et al. tested the pore water pressure of sand and silty clay under freeze thaw cycling and observed that its decrease is the primary driving force of water migration during freezing [4]. Furthermore, the pore water pressure mostly depends on the temperature, freeze thaw history, and soil type. Ren et al. experimentally measured the resilient modulus of five soil types popularly used as subgrade and sidewalk under wetting and freeze thaw conditions [5]. The resilient modulus at the optimum water content significantly decreased under critical freeze thaw cycling. Chen et al. conducted freeze thaw cycling tests at different temperatures and times on the remodeled samples of silty clay from a seasonal frozen area [6]. They assessed the pore structure under different test conditions using the mercury injection method. They combined these results with the fractal theory to explore the influence of freezing temperature and freeze thaw cycling time on pore structure variation in silty clay. Li et al. performed fifteen freeze thaw cycles on four groups of sandstone samples under graded loading while measuring the pore variation via nuclear magnetic resonance (NMR) and studying their creep mechanical properties [7]. The results demonstrated decreased cohesion between the rock particles, deteriorated pore structure, and increased porosity after freeze thaw cycling. Rui et al. made an L-shaped retaining wall using broken glass and expanded polystyrene as back-filling materials, observing the freezing front, ground temperature, and wall deformation in its back-filling soil during three freeze thaw seasons and demonstrated the suitability of

granular waste for frost heave prevention [8]. He et al. conducted direct shear tests during freeze thaw cycles at different temperatures and times to examine their influence on the shear performance of the interface between frozen soil and concrete [9]. The results attributed this influence to the water migration to the interface and the formation and accumulation of an ice film. The peak displacement linearly increased along with the initial water content; however, its correlation decreased at a higher number of freeze thaw cycles. Therefore, domestic and foreign researchers have demonstrated that the mechanical properties of frozen soil and the phenomenon of frost heave and thaw subsidence depend on the hydrothermal migration and phase transition in frozen ground, which is importantly the coupling problem of water–heat–force–deformation in porous multiphase media.

During freeze thaw cycles, the role of supporting structures in soil is affected. Mo and Lou simulated the frost heaving of a concrete channel lining using a multifield coupling software and examined the frost heave distribution in the structure of the channel lining and the substrate soil of the composite geomembrane [10]. The composite geomembrane under the lining could reduce the frost heave of the foundation soil to some extent. Yuan et al. determined the parameters of a slope anchoring system, such as anchoring force, displacement, anchor stress, and bond strength between grouted rock bolts and cement mortar using a physical simulation [11]. They examined the deterioration in the bond and anchor performance of the bolts under freeze thaw conditions. The maximum anchor stress was observed in the middle of the bolts, where shear failures, which is caused by a reduction in the strength and stiffness of the cement mortar, leads to bonding ability loss possibly occurring. Hu monitored a prestressed anchor support structure and the secondary development of frozen soil materials, established a similar model for a deep foundation pit, and examined the evolution of stress and deformation during overwintering [12]. Cui et al. performed freeze thaw cycling tests on a 1 m-high geogrid-reinforced retaining wall under different loadings [13]. The experimental results demonstrated the influence of the ambient temperature and the number of freeze thaw cycles on its temperature field and mechanical properties. Moreover, its performance primarily changed after the first two–three cycles [14–16]. The top subsidence and lateral displacement of the retaining wall increased along with the number of freeze thaw cycles [17–20].

A few studies investigated the supporting performance of prestressed anchor cables in the deep foundation pits of subway stations during spring thaw in cold regions [20–24]. The evolution law of the deformation of supporting piles and the axial force of prestressed anchor cables requires to be clarified. This leads to a lack of scientific guidance for designing prestressed pile anchor systems for deep foundation pits in cold freeze thaw regions [25–29]. Northeast China is an alpine area, and it presents seasonally frozen soil. Therefore, this study focused on the deep foundation pit project for a subway station in Changchun as an example of a prestressed pile anchor supporting system during the spring thaw. Field monitoring and numerical simulations were combined considering the thermal–mechanical coupling effect. This study examined the performance of the selected prestressed pile anchor system and its variation under freeze thaw conditions.

2. Deep Foundation Pit Project

The development of the subway station in Changchun investigated in this study uses a combination of open and covered excavation. The length, width, and excavation depth of the foundation pit in the open excavation section are 240.5, 22.9, and 19.7 ~ 20.1 m. Table 1 presents the soil layer information for the 60 m depth range in the foundation pit area. Changchun is in a moderate-temperate zone with a subhumid/semiarid monsoon climate in the midtemperate continental area, and its spring melt period is from March to May.

The foundation pit supporting structure comprises five prestressed anchor cables between the piles from top to bottom. The diameter, length, and spacing of the bored perfusion piles are 800 mm, 25 m, and 1.3 m, respectively. The prestressed anchor cables are anchored into the stable rock and soil mass of the site, and their free section is fixed between the supporting piles with anchors. The horizontal spacing of anchor cables is 1.3 m, and the foundation pit structure is shown in Figure 1. Furthermore, the design parameters of the prestressed anchor cables are shown in Table 2.

The surface subsidence of the bottomless foundation pit was monitored from March to June 2021 at 2, 5, and 8 m from the excavation surface, with a frequency of 24 h. The monitoring points are shown in Figure 2. Measuring points 1 and 2 are located at the north and south sides of the foundation pit and are 2, 5, and 8 m away from the free surface and are denoted as $LS(1/2) - (N/S) - (2/5/8)$.

3. Three-Dimensional Numerical Model

3.1. Model Size. As per Saint-Venant's principle and the subway station's actual size, the 3D numerical model's length was 182.5 m. Four supporting piles and their spacing were considered in the width direction, corresponding to the width set at 5.2 m. The height was set at 60 m. The diameter and length of the piles were 0.8 m and 25 m. The crown beam was 1 m high because it was considered a part of the piles. Their length was 26 m with a spacing of 1.3 m.

The retaining pile was simplified as an equal-thickness diaphragm wall to facilitate the numerical calculation and based on the principle of equivalent flexural stiffness. The resulting thickness of the equivalent ground-connecting wall was 0.486 m. The shooting angle of the anchor cable is 14°. The model is schematized in Figures 3 and 4.

3.2. Material Parameters. A coupled eight-node trilinear displacement–pore pressure–temperature element (C3D8PT) with a modified DP model was adopted. For the equivalent ground-connecting wall, a coupled eight-node trilinear displacement–temperature element (C3D8T) with an elastic model was used, while a two-node beam element (B31) and an elastic model were selected for the prestressed anchor cables. The density, Poisson's ratio, elastic modulus, and

Table 1: Soil layer information of the foundation pit project.

Name of the soil type	Thickness/m
Miscellaneous fill	1.1
Silty clay fill	4.8
Silty clay①	5.8
Silty clay②	5.5
Fully weathered sandstone	2.4
Strongly weathered mudstone	6.1
Moderately weathered mudstone	34.3

expansion coefficient were 7693 kg/m^3, 0.3, 195 GPa, and 1 $\times 10^{-5}$ W/$(m \cdot K)$.

The calculated material parameters are summarized in Table 3. The ground-connecting wall, anchor cables, and foundation pit were constructed using the birth and death element method. The soil and ground-connecting wall were in face-to-face contact, and the normal behavior was set as hard contact. The free end of the prestressed anchor cables was connected using the ground-connecting wall by binding constraints, and the anchorage section was connected with the stable soil via embedded constraints.

3.3. Simulation Steps. The specific times and tasks of analysis steps are shown in Table 4. The temperature simulation of drxh1 and drxh4 steps was based on proper temperature values during the annual cycle. Because of the large average daily temperature difference during freeze and thaw, the most obvious freeze thaw cycle in the early spring thaw period, which exhibited the largest daily temperature difference, was divided into three stages (drxh2-1, drxh2-2, and drxh2-3). However, the middle and late spring thaw periods were considered as one stage (drxh3).

3.4. Boundary Conditions and Loads. The displacement constraints in the normal direction were set on the side and bottom edges of the model. The drainage boundary was the exposed surface of the soil body, excluding the ground-connecting wall after foundation pit excavation (top and bottom surface of the foundation pit and wall–soil contact surface), and its pore pressure was set as 0. The soil saturation and initial temperature were set as 1 and 6.4°C, respectively. The temperature boundary condition was set on the top surface of the soil to simulate geothermal equilibrium for five years, and the simulation result was used as the initial temperature field calculated by the model.

The gravity load was applied to the entire model, and the vertical gravity acceleration was 9.8 m/s^2. The mechanical response of the model under gravity load was calculated. To simulate the ground load around the foundation pit, a uniform load of 20 kPa was applied to the surface at 1 m from the foundation pit surface. The temperature boundary conditions were set from the freeze thaw stage after the completion of construction. The temperature boundary that is the foundation pit is the top surface of the free surface and bottom surface of the foundation pit. The temperature function was obtained by fitting the annual average and daily temperature changes during the spring melt period (March to June) in Changchun (Table 5) .

3.5. Model Verification. To confirm the reliability of the numerical model, the simulated surface subsidence during spring thaw was compared with the corresponding monitoring data (Figure 5), revealing a wide gap of 20%. The difference in the monitoring values for both sides of the foundation pit was primarily attributed to the different light intensity, material load, and construction steps, while the failure of the monitoring data to demonstrate apparent melting and subsidence might have been caused by earthwork excavation and other construction factors. The calculated subsidence value at 2 m from the excavation surface was more significant than the corresponding monitoring value on both excavation sides during the spring thaw.

The primary reasons were as follows: a concrete pavement was constructed on both sides of the excavation site but was not considered in the simulation. The numerical simulation of surface subsidence was more sensitive to temperature than the actual site. The concrete pavement had a specific limiting effect on the frozen uplift and thawing subsidence of the soil. The concrete pavement between 5 and 8 m from the free surface of the foundation pit was less affected, and the corresponding calculated subsidence values were consistent with the monitoring ones on both foundation pit sides. A comprehensive comparison of surface subsidence calculations and monitoring results revealed consistency with the former ones under the change law.

In terms of the anchor cable axial force, the calculated and monitored values were within a 20% error, and the simulation results were basically at the same level as the monitoring results (Figure 6). The difference in the monitored axial force values on both pit sides was primarily attributed to the different light intensities, material loading, and construction steps. The fifth of the five anchor cables demonstrated the most significant difference between calculated and monitored axial force. This occurred primarily because the soil and water pressures, in addition to the tensile force on the prestressed anchor cable, were greater at the pit bottom than at the top. Moreover, most of the calculated axial force values demonstrated a more consistent variation pattern than the monitoring ones. The axial force gradually mostly following a relatively slow decreasing trend at the middle and end of spring melt. A comparison between simulation and monitoring results demonstrated that the numerical model could be considered reliable, and the calculation results are promising.

4. Simulation Results and Discussion

4.1. Surface Subsidence. Figure 7 shows the changes in surface subsidence during spring thaw at 2, 5, and 8 m from the free surface of the foundation pit, thus demonstrating the same trend regardless of the distance. When the daily average temperature never rose > 0 during the early spring thaw period, the surface upliftment occurred in all three places, and the surface subsidence demonstrated a decreasing trend. Around March 15 (the first and second stages of

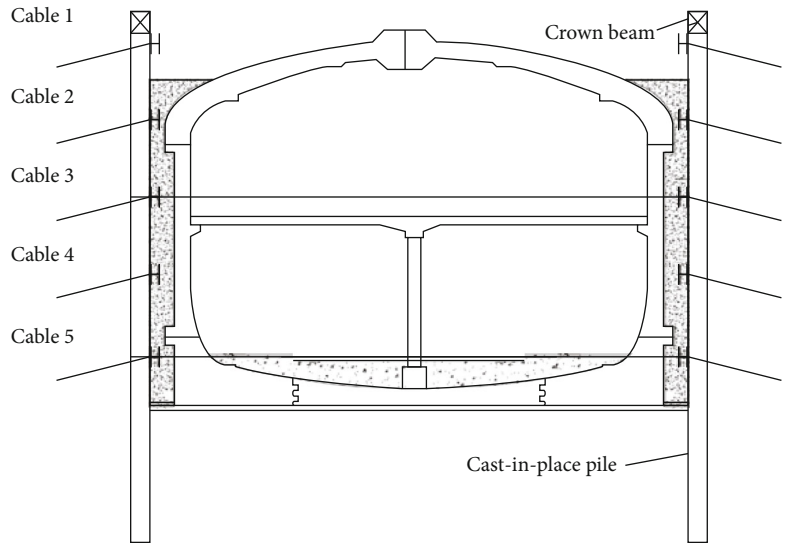

Figure 1: Section of the foundation pit.

Table 2: Design parameters of the prestressed anchor cables.

Anchor cable	Length/m Total length	Anchorage section	Free section	Steel strand	Standard value of axial force/kN	Preaxial force/kN
Cable 1	21.0	13.0	8.0	$3\times7\varphi S13.5$	77.8	60
Cable 2	23.0	16.0	7.0	$3\times7\varphi S13.5$	169.8	122
Cable 3	27.0	20.0	7.0	$5\times7\varphi S13.5$	329.1	244
Cable 4	24.0	17.0	7.0	$6\times7\varphi S13.5$	453.1	325
Cable 5	15.0	10.0	5.0	$5\times7\varphi S13.5$	312.0	256

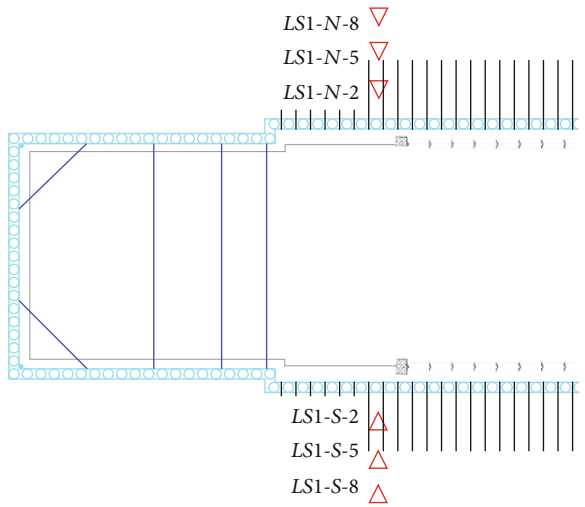

Figure 2: Schematic of monitoring points.

the early spring thaw), the surface subsidence reached the minimum value. After a few days of stability, surface subsidence became visible on March 20 in all three places, and it gradually increased because the daily average temperature exceeded zero. The subsidence growth rate was the fastest in the middle stage of the spring thaw and relatively slow in the middle and late stages. However, during the entire spring thaw period, the subsidence at 2 m from the free surface was the largest, followed by that at 5 and 8 m, consistent with the monitoring data. In the early spring thaw, the settlement growth rate at 8 m from the free surface of the foundation pit was the highest. In the middle and late stages of the spring thaw, the subsidence growth rate was greater at 2 and 5 m.

4.2. Anchor Cable Axial Force. In the first stage of the early spring thaw, the temperature was low, and the duration of the favorable temperature was short. Most frozen layers' daily thawing and refreezing were extremely small and basically equivalent. The supporting piles would exhibit a slight rebound trend when there is a certain amount of thawing in the free surface soil. However, because the frost heaving force of the soil at the surface bottom will weaken a little at this stage, the overall rebound of the supporting piles would slightly exceed the deformation at this stage. Hence, the axial force of the last four anchor cables slowly decreased. The anchor point of the first cable on the supporting pile was located at the external corner of the foundation pit (two-way interaction between the temperatures at

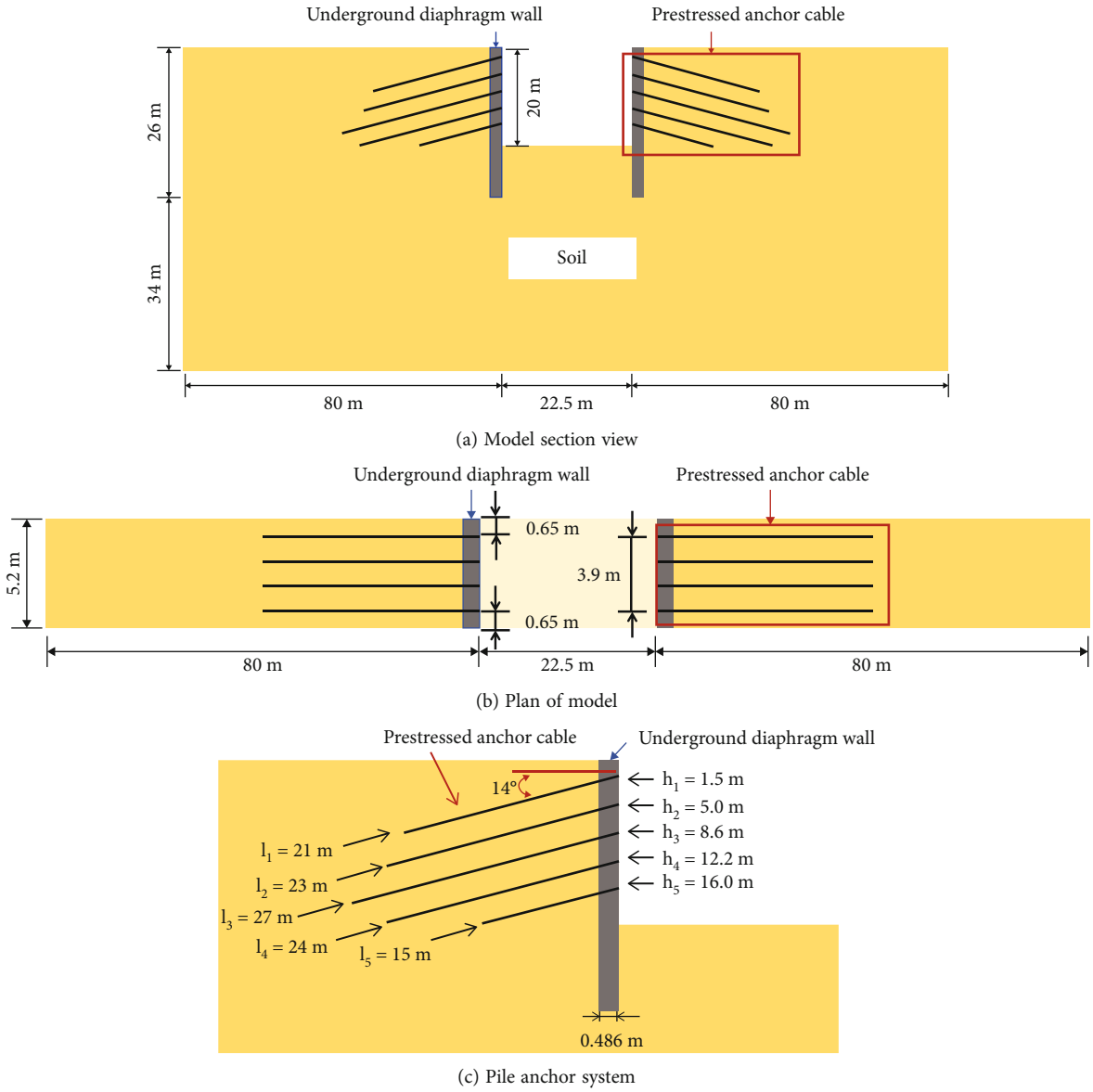

Figure 3: Simplified schematic of the 3D numerical model.

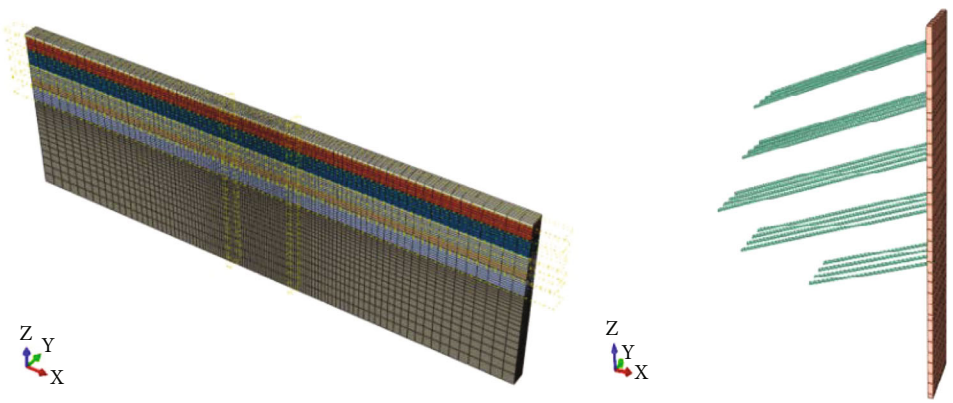

Figure 4: 3D numerical model.

Table 3: Material parameters.

Serial number		Density ρ/(kg/m^3)	Poisson's ratio ν	Elasticity modulus E/MPa	Conductivity λ/[W/(m·K)]	Specific heat c/[J/(kg·K)]	Permeability k/(m/s)	Internal friction angle/°	Cohesion force/kPa
	1	1850	0.30	10	1.61	1510	2.0E-6	24.1	39.94
	2	1950	0.30	25.2	1.62	1520	3.6E-6	24.1	52.56
	3	1980	0.29	27.2	1.44	1670	5.8E-6	27.8	54.89
No.	4	2020	0.26	46.8	1.71	1440	4.6E-6	27.8	65.45
	5	1970	0.25	40	1.55	1250	5.8E-5	29.5	52.87
	6	2110	0.24	120	1.37	1060	3.5E-6	44.5	105.55
	7	2130	0.21	160	1.42	1120	9.7E-6	54.8	243.32
Underground diaphragm wall		2500	0.2	31000	1.74	920	—	—	—

Table 4: Simulation steps.

Stage	Serial number	Name	Duration/s	Task
Construction phase	1	Addwall	1	Construction of diaphragm wall (supporting piles)
	2	kw1	1	First earthwork excavation (2.0 m)
	3	addms1	1	First anchor line construction (1.5 m)
	4	kw2	1	First anchor line construction (5.5 m)
	5	addms2	1	Second anchor cable construction (5.0 m)
	6	kw3	1	Third earthwork excavation (9.1 m)
	7	addms3	1	Third anchor cable construction (8.6 m)
	8	kw4	1	Fourth earthwork excavation (12.7 m)
	9	addms4	1	Fourth anchor cable construction (12.2 m)
	10	kw5	1	Fifth earthwork excavation (16.5 m)
	11	addms5	1	Fifth anchor cable construction (16.0 m)
	12	kw6	1	Sixth earthwork excavation (20.0 m)
Freezing and thawing phase	13	drxh1	151×86400	Before spring thaw (after October 1)
	14	drxh2-1	15×86400	First stage of early spring melt
	15	drxh2-2	15×86400	Second stage of early spring melt
	16	drxh2-3	10×86400	Third stage of early spring melt
	17	drxh3	82×86400	Middle and late spring melt
	18	drxh4	92×86400	After spring thaw (ends September 30)

Table 5: Temperature function.

Type	Serial number	Expression of temperature function	Action stage	Operation duration and corresponding time
Type 1	Tem1	$T_1 = 5 - 2 \cdot \cos \omega 1t - 18.89 \cdot \sin \omega 1t$ $T_2 = 5 + 18.91 \cdot \cos \omega 1t - 1.76 \cdot \sin \omega 1t$ $(-14 \circ \mathrm{C} \le T \le 24 \circ \mathrm{C})$	Before the spring melting T_1 Before the spring melting T_2	Before the spring melting:151days (10.1~2.28) After the spring melt:92days (7.1~9.30)
Type 2	Tem2	$T = -12 \cdot \cos \omega 2t$ $(-12 \circ \mathrm{C} \le T \le 12 \circ \mathrm{C})$	The first stage of early spring melt	15 days (3.1~3.15)
	Tem3	$T = 5 - 11 \cdot \cos \omega 2t$ $(-6 \circ \mathrm{C} \le T \le 16 \circ \mathrm{C})$	The second stage of early spring melt	15 days (3.16~3.30)
	Tem4	$T = 8 - 12 \cdot \cos \omega 2t$ $(-4 \circ \mathrm{C} \le T \le 20 \circ \mathrm{C})$	The third stage of early spring melt	10 days (3.31~4.9)
	Tem5	$T = 14 - 10 \cdot \cos \omega 2t$ $(4 \circ \mathrm{C} \le T \le 24 \circ \mathrm{C})$	Middle and late spring melt	82 days (4.10~6.30)

Note: In the table, $\omega_1 = 1.99238 \times 10 - 7$; $\omega_2 = 7.27221 \times 10 - 5$.

the top and the free surface of the foundation pit). The frost heaving effect in this area was most apparent during the freezing period and more affected by temperature in early spring thaw than the lower soil mass of the free surface. In the early spring thaw, the freeze thaw cycle occurred in this area, causing microsoil cracks. Generally, the soil mass forms large pores after the ice crystals melt. Because the thawing of the lower soil mass of the free surface was minimal in the early spring thaw, and the void ratio of the soil mass at the external corner of the foundation pit increased because of the freeze thaw cycle, the surface soil mass remained at the bottom of this outer corner after the thawing water partially seeped. However, the seeping did not continue, and the soil mass refreezing at the first anchor cable anchorage was more significant than the thawing in the early spring thaw. Therefore, the axial force at the beginning of spring thaw exceeded that of the second anchor cable, and it tends to increase at the beginning of the spring thaw.

In the second and third stages of the early spring thaw, the overall freeze thaw cycle of the frozen layer of soil was significant. The overall melting of the soil mass started to be greater than the refreezing. However, the continuous infiltration of melted water made the freeze thaw cycle effect of the lower soil mass of the free surface more prominent.

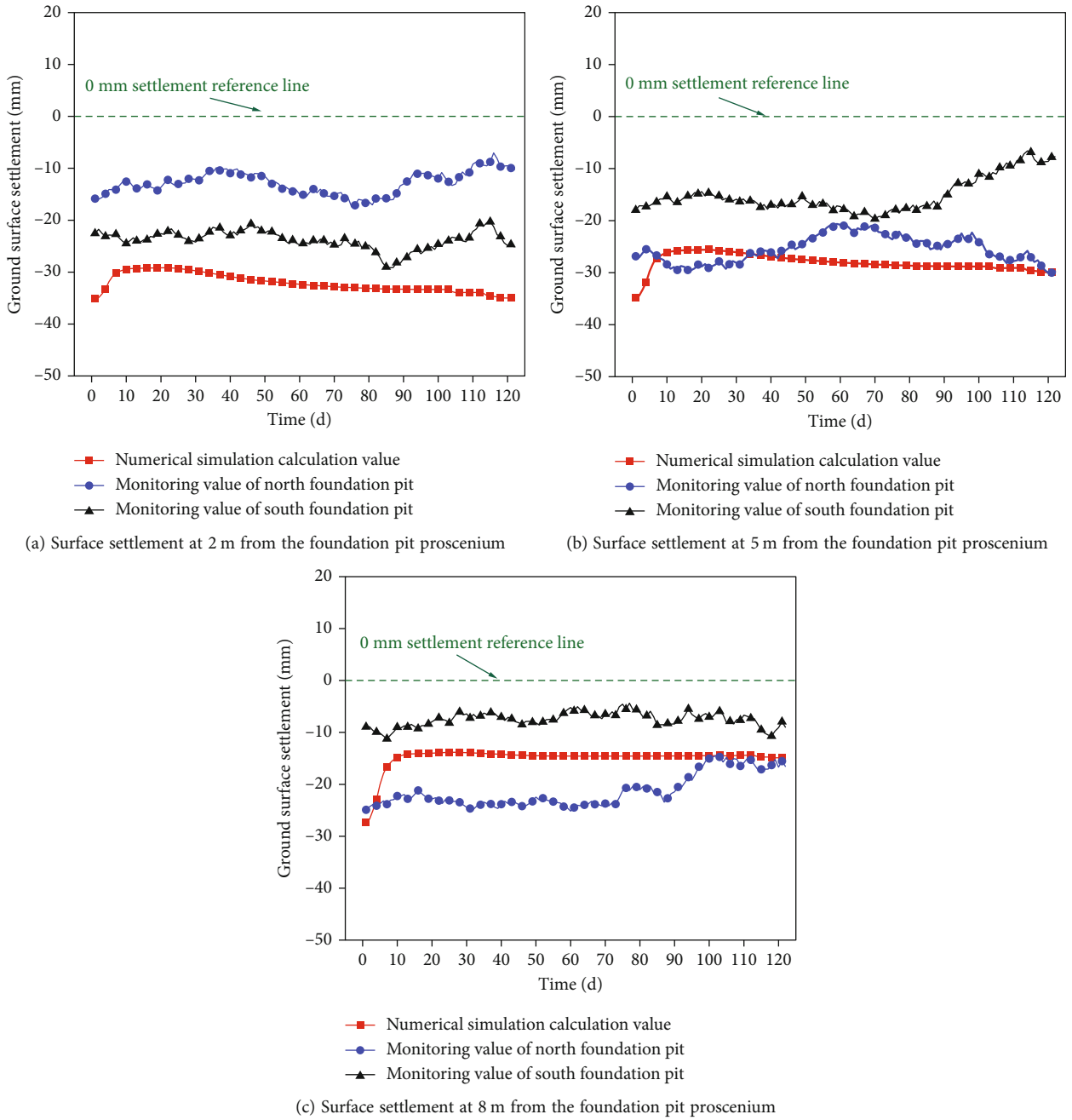

(a) Surface settlement at 2 m from the foundation pit proscenium

(b) Surface settlement at 5 m from the foundation pit proscenium

(c) Surface settlement at 8 m from the foundation pit proscenium

Figure 5: Comparison of surface settlement simulation results and monitoring results.

The freeze thaw cycle refreezing was enhanced and decreased extremely slowly. The frost heaving force on the lower part of the cantilever section of the supporting piles gradually increased. Hence, the axial force of the last four anchor cables began to increase. Moreover, with the continuous infiltration of the upper layer of melted water, the increasing trend of the anchor cable axial force became more obvious, and the duration was longer. The infiltration of thawing water reduced the refreezing of the soil behind the top of the retaining pile during the freeze thaw cycle, and the frost heaving force on that section began to decrease. Therefore, the axial force of the first anchor cable gradually decreased in the second and third stages of the early spring thaw.

In the late stages of the spring thaw, the soil entirely began to melt, the frozen layer thickness decreased, the shallow frozen layer completely melted, the frost heaving force on the supporting pile gradually disappeared, and the water and soil pressure behind the supporting piles and their horizontal displacement tended to be stable. The prestressed anchor cable presented gradually decreasing trend as shown in Figure 8.

4.3. Pile Horizontal Displacement. Figure 9 shows the variation in the pile's horizontal displacement with depth during the spring thaw. The horizontal displacement gradually increased from bottom to top along the pile length, and its

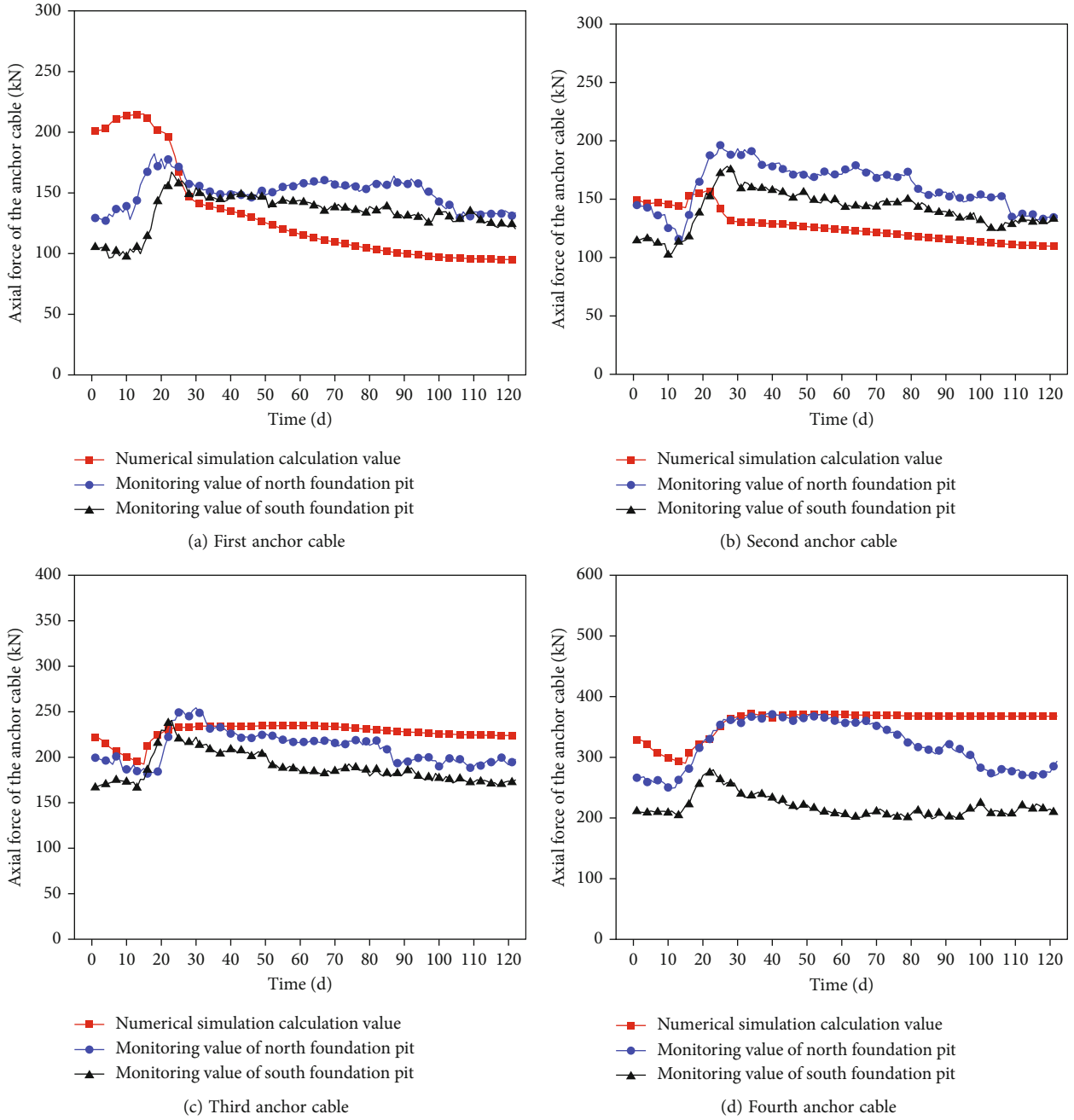

Figure 6: Continued.

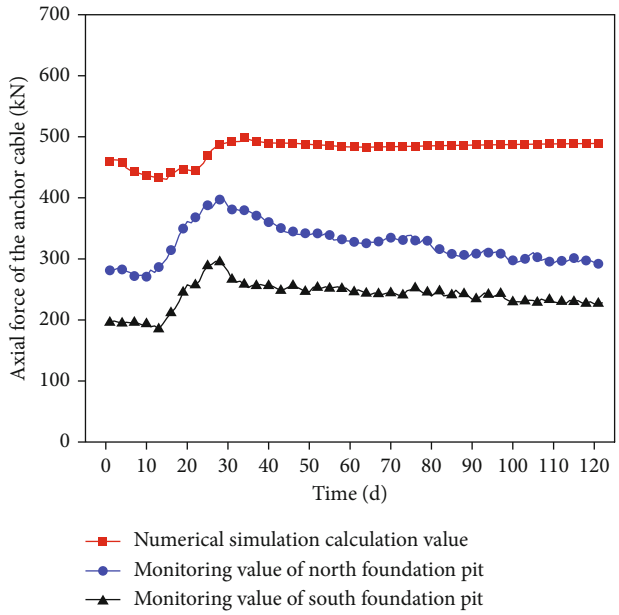

(e) Fourth anchor cable

Figure 6: Comparison between simulation and monitoring results about the axial force of the anchor cables.

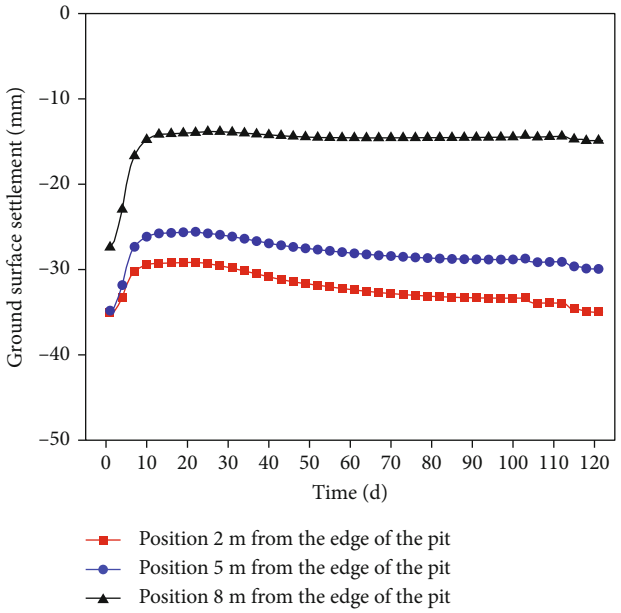

Figure 7: Variation in surface subsidence during spring thaw.

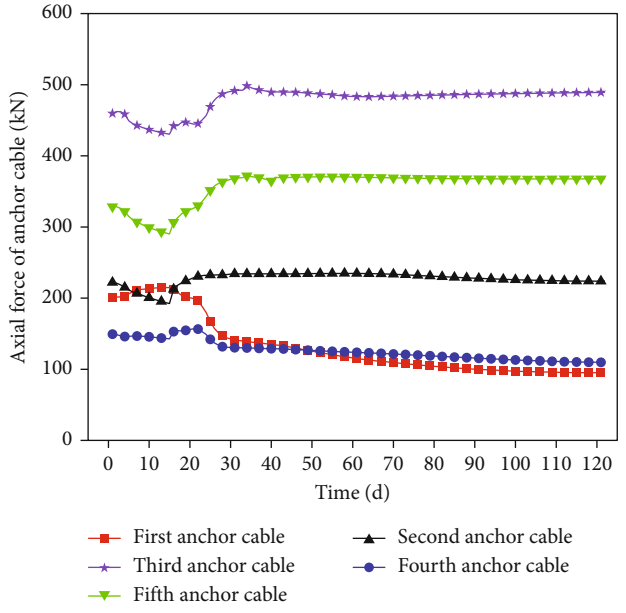

Figure 8: Changes in the axial force of the prestressed anchor cables during spring thaw.

variation span (horizontal displacement difference) was significant for the lower part of the piles. The horizontal displacement below the anchorage point of the fifth anchor cable varied over a large span, while it changed only a little above that anchorage point. This indicates that the prestressed anchor cable shared part of the load with the pile, thus limiting the horizontal displacement of its cantilever section.

From March 15 to April 1, the horizontal displacement of the pile continuously increased (Figures 9(b)–9(d). During this time, it changed the most from March 21 to March 26. This suggests that the frozen layer of soil behind the piles and at the pit bottom had been subjected to different degrees of freeze thaw cycles during the early spring thaw period, causing the soil pressure, freeze thaw force, and anchor cable axial force to change at different depths during the spring thaw. It resulted in different magnitudes of postpile pressure and pile bending moments as per the pile depths, which ultimately affected the pile deformation at different depths.

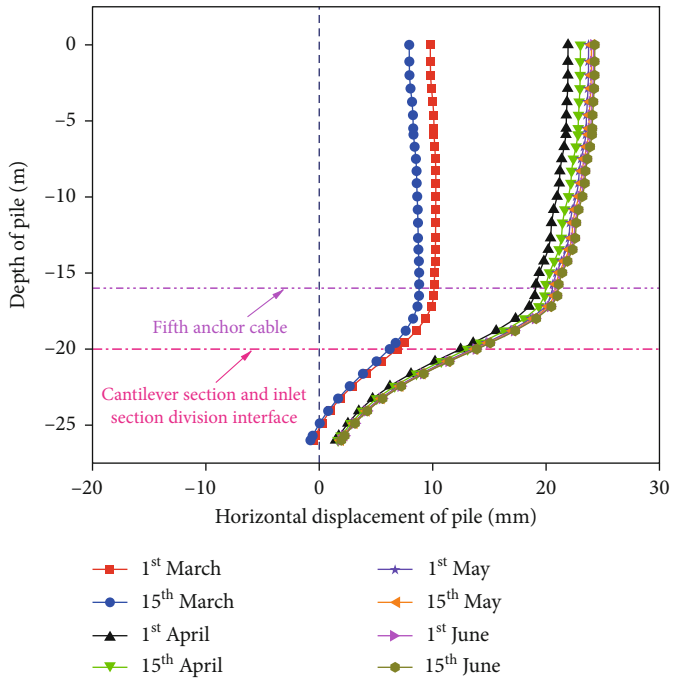

(a) Spring thaw period

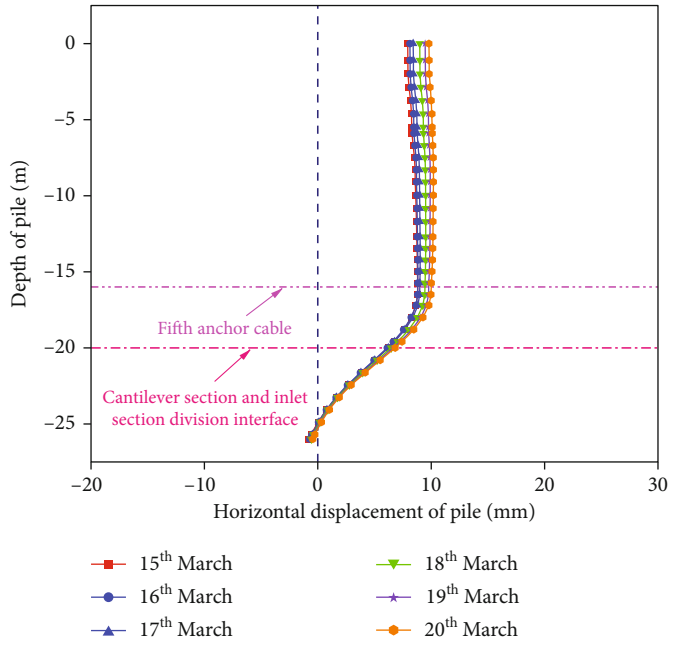

(b) 15th March to 20th March

Figure 9: Continued.

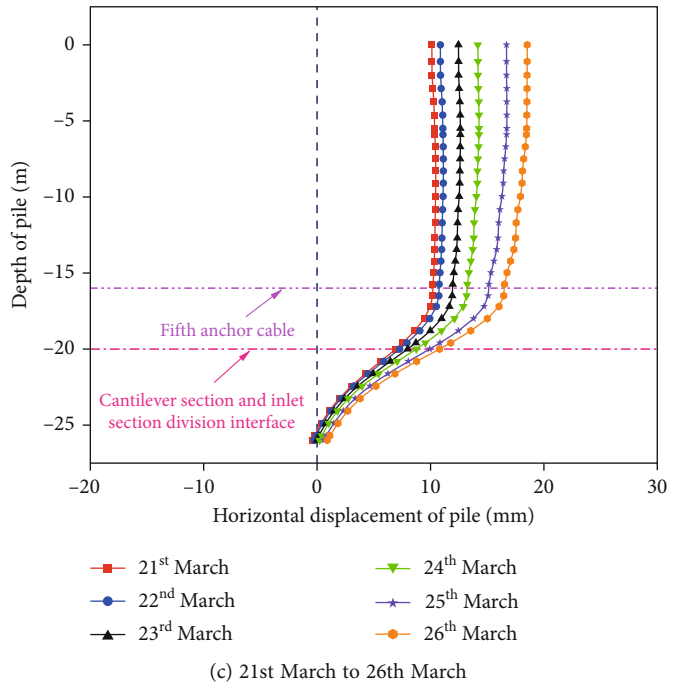

(c) 21st March to 26th March

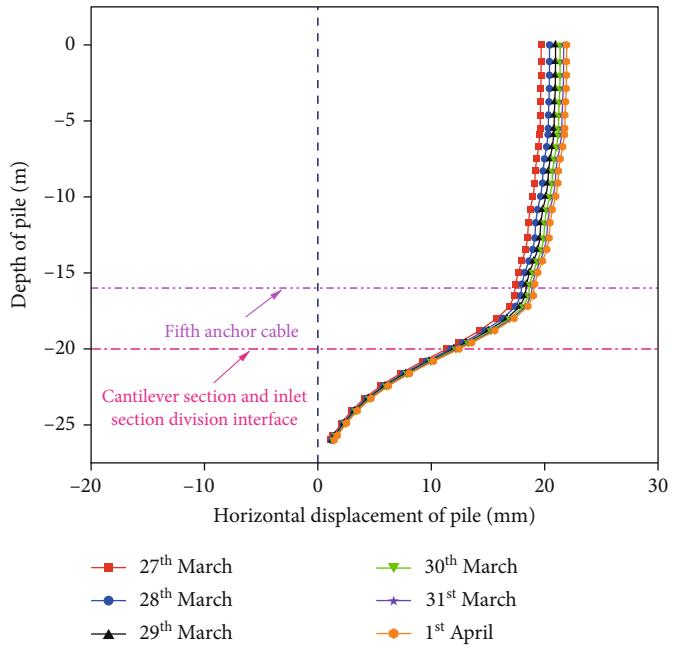

(d) 27th March to 1st April

Figure 9: Variation in the pile horizontal displacement during the spring thaw.

5. Conclusions

A complete simulation was performed to examine the mechanical behavior of the prestressed pile anchor system of a typical deep foundation pit during spring thaw using a 3D water–heat–mechanical coupling model. After the model validation with relevant monitoring data, the variation rules of the surface subsidence, anchor cable axial force, and pile horizontal displacement during the spring thaw were analyzed, thus leading to the following results.

(1) During the early spring thaw, the ground surface at 2, 5, or 8 m from the pit excavation surface tended to rise. The subsidence phenomenon first appeared during the second stage of the early spring thaw (when the average temperature rose above 0°C), and the subsidence growth rate was peaked during the middle stage of the spring thaw period

(2) During the early spring thaw, the axial force of the first to fifth anchor cables gradually decreased with

a slowling tendency in the middle and late stages. The axial force of the first anchor cable changed earlier than the other cables, increasing first and then decreasing during the early spring thaw

(3) The horizontal displacement of the pile body could be roughly divided into three stages during the spring thaw. In the first stage, there was a rebound trend, which was the largest for the cantilever section. The horizontal displacement exhibited the most significant variation in the second stage. In the third stage, it increased but with a minor variation

Data Availability

The data used to support the findings of this study are included in the article.

Conflicts of Interest

The authors declare that they have no conflicts of interest.

Acknowledgments

This research was supported by the research project on planning of holistic and systematic approach for conserving and restoring mountain, water, forest, farmland, grassland, and desert ecosystems in the Lijiang river basin of Guilin city (Grant No. GLZC2019-G3-00897-KWZB).

References

[1] B. Chen and J. P. Li, "Characteristics of spatial and temporal variation of seasonal and short-term frozen soil in China in recent 50 years," *Chinese Journal of Atmospheric Sciences*, vol. 32, no. 3, pp. 432–443, 2008.

[2] L. Geng, S. Cong, J. Luo, X. Ling, X. du, and Y. Yu, "Stress–strain model for freezing silty clay under frost heave based on modified Takashi's equation," *Applied Sciences*, vol. 10, no. 21, p. 7753, 2020.

[3] R. L. Shi, *Study on Influence of Frost Heaving Effect on Retaining and Protection for Excavations of Soil Nailing Wall in Seasonal Frozen Zone*, Jilin Jianzhu University, 2019.

[4] L. Zhang, W. Ma, and C. Yang, "Investigation on the effects of freeze-thaw action on the pore water pressure variations of soils," *Journal of Offshore Mechanics and Arctic Engineering*, vol. 140, no. 6, pp. 1–5, 2018.

[5] J. Ren, S. K. Vanapalli, Z. Han, K. O. Omenogor, and Y. Bai, "The resilient moduli of five Canadian soils under wetting and freeze-thaw conditions and their estimation by using an artificial neural network model," *Cold Regions Science and Technology*, vol. 168, article 102894, 2019.

[6] Z. Chen, H. Chen, J. Li, H. Li, and W. Ma, "Study on the changing rules of silty clay's pore structure under freeze-thaw cycles," *Advances in Civil Engineering*, vol. 2019, Article ID 7493872, 2019.

[7] J. Li, L. Zhu, K. Zhou, S. Cao, and H. Liu, "Experimental investigation on the effects of ambient freeze-thaw cycling on creep mechanical properties of sandstone under step loading," *IEEE Access*, vol. 2019, no. 7, pp. 108513–108520, 2019.

[8] D. Rui, H. Deng, D. Nakamura, S. Yamashita, T. Suzuki, and H. Zhao, "Full-scale model test on prevention of frost heave of L-type retaining wall," *Cold Regions Science and Technology*, vol. 132, pp. 89–104, 2016.

[9] P. He, Y. Mu, Z. Yang, W. Ma, J. Dong, and Y. Huang, "Freeze-thaw cycling impact on the shear behavior of frozen soil-concrete interface," *Cold Regions Science and Technology*, vol. 2019, article 103024, no. 173, 2019.

[10] T. Mo and Z. Lou, "Numerical simulation of frost heave of concrete lining trapezoidal channel under an open system," *Water*, vol. 12, no. 2, p. 335, 2020.

[11] J. Yuan, C. Ye, J. Yang et al., "Experimental and numerical investigation on the deterioration mechanism for grouted rock bolts subjected to freeze-thaw cycles," *Bulletin of Engineering Geology and the Environment*, vol. 80, no. 7, pp. 5563–5574, 2021.

[12] Y. Hu, *Study on the Performance of Prestressed Anchor Support Structure of Deep Foundation Pit in Alpine and Deep Season Permafrost Area*, Harbin Institute of Technology, 2021.

[13] F. Cui, C. Xiao, J. Han, S. Gao, and W. Tian, "Performance of laboratory geogrid-reinforced retaining walls under freeze-thaw cycles," *Geosynthetics International*, vol. 29, no. 1, pp. 81–98, 2022.

[14] X. Chen, X. Jin, Y. Guan, S. Zhuo, and G. Yi, "The influence of daily and annual variation of the surface temperature on near-surface temperature survey," *Progress in Geophysics*, vol. 21, no. 3, pp. 1008–1011, 2006.

[15] S. Cong, L. Tang, X. Ling et al., "Three-dimensional numerical investigation on the seepage field and stability of soil slope subjected to snowmelt infiltration," *Water*, vol. 13, no. 19, p. 2729, 2021.

[16] F. Tong, L. Gao, X. Cai, Y. Zhong, W. Zhao, and Y. Huang, "Experimental and theoretical determination of the frost-heave cracking law and the crack propagation criterion of slab track with water in the crack," *Applied Sciences*, vol. 9, no. 21, p. 4592, 2019.

[17] W. Nie, W. Wang, Z. Tao, C. Zhu, and Y. Chen, "Numerical modeling of the NPR-cable and its applications for analysis of a slide-toe-toppling failure," *Computers and Geotechnics*, vol. 149, article 104852, 2022.

[18] C. Zhu, Z. Yan, Y. Lin, F. Xiong, and Z. Tao, "Design and application of a monitoring system for a deep railway foundation pit project," *IEEE Access*, vol. 7, article 107591, 2019.

[19] C. Zhu, K. Zhang, H. Cai et al., "Combined application of optical fibers and CRLD bolts to monitor deformation of a pit-in-pit foundation," *Advances in Civil Engineering*, vol. 2019, Article ID 2572034, 16 pages, 2019.

[20] Q. Wang, S. Xu, Z. Xin, M. He, H. Wei, and B. Jiang, "Mechanical properties and field application of constant resistance energy- absorbing anchor cable," *Tunnelling and Underground Space Technology*, vol. 125, article 104526, 2022.

[21] Q. Wang, B. Jiang, S. Xu et al., "Roof-cutting and energy-absorbing method for dynamic disaster control in deep coal mine," *International Journal of Rock Mechanics and Mining Sciences*, vol. 158, article 105186, p. 105186, 2022.

[22] M. He, Q. Sui, M. Li, Z. Wang, and Z. Tao, "Compensation excavation method control for large deformation disaster of mountain soft rock tunnel," *International Journal of Mining Science and Technology*, vol. 32, no. 5, p. 951, 2022.

[23] W. Zhao, J. Han, Y. Chen et al., "A numerical study on the influence of anchorage failure for a deep excavation retained

by anchored pile walls," *Advances in Mechanical Engineering*, vol. 10, no. 2, Article ID 168781401875677, 2018.

[24] L. Tang, Z. H. Cheng, X. Z. Ling, S. Cong, and J. Nan, "Preparation and performance of graphene oxide/self-healing microcapsule composite mortar," *Smart Materials and Structures*, vol. 31, no. 2, article 025022, 2022.

[25] Z. H. Cheng and Y. S. Deng, "Bearing characteristics of moso bamboo micropile-composite soil nailing system in soft soil areas," *Advances in Materials Science and Engineering*, vol. 2020, Article ID 3204285, 2020.

[26] Y. Deng, Z. Cheng, M. Cai, Y. Sun, and C. Peng, "An experimental study on the ecological support model of dentate row piles," *Advances in Materials Science and Engineering*, vol. 2020, Article ID 6428032, 2020.

[27] J. Y. Han, W. Zhao, Y. Chen, P. J. Jia, and Y. P. Guan, "Design analysis and observed performance of a tieback anchored pile wall in sand," *Mathematical Problems in Engineering*, vol. 2017, Article ID 8524078, 2017.

[28] J. Han, D. Liu, Y. Guan et al., "Study on shear behavior and damage constitutive model of tendon-grout interface," *Construction and Building Materials*, vol. 320, article 126223, 2022.

[29] Y. Chen, W. Zhao, P. Jia, and J. Y. Han, "Proportion analysis of ground settlement caused by excavation and dewatering of a deep excavation in sand area," *Indian Geotechnical Journal*, vol. 48, no. 1, pp. 103–113, 2018.